

A multi-wavelength study of nearby starburst galaxy M 82

Nilkanth Vagshette^{1*}, Satish Sonkamble^{2*}, Madhav Patil³,
Sachindra Naik⁴, Ilani Loubser^{2,5}

¹Department of Physics and Electronics, Maharashtra Udayagiri Mahavidyalaya, Udgir, 413517, Maharashtra, India.

²Centre for Space Research, North-West University, Potchefstroom, 2520, North West, South Africa.

³School of Physical Sciences, Swami Ramanand Teerth Marathawada University, Street, Nanded, 431606, Maharashtra, India.

⁴Astronomy & Astrophysics Division, Physical Research Laboratory, Ahmedabad, 380009, Gujarat, India.

⁵National Institute for Theoretical and Computational Sciences (NITheCS), Potchefstroom, 2520, North West, South Africa.

*Corresponding author(s). E-mail(s): nilkanth1384@gmail.com;
satish04apr@gmail.com;

Abstract

We present a multi-wavelength study of the nearby starburst galaxy M 82 by combining high-resolution Far-ultraviolet (FUV) imaging from the Ultra-Violet Imaging Telescope (UVIT) onboard AstroSat and archival *Chandra* X-ray observations. Using FUV flux measurements, we estimate a spatially-resolved star formation rate (SFR) across several star-forming clumps within a radius of ~ 3.6 kpc, finding a total SFR of $0.022 M_{\odot} \text{ yr}^{-1}$. The H_{α} recombination line flux yields an SFR of $\sim 0.010 M_{\odot} \text{ yr}^{-1}$, while the infrared-based SFR derived from $24 \mu\text{m}$ emission is significantly higher at $16 - 18 M_{\odot} \text{ yr}^{-1}$, suggesting that a substantial fraction of star formation in M 82 is heavily dust-obscured. Morphological comparison of FUV, H_{α} , mid-infrared, and soft X-ray emission reveals a strong spatial correlation, tracing multi-phase outflows along the galaxy's minor axis. X-ray spectral analysis using a three-temperature VAPEC model shows enhanced abundances of Ne, Mg, Si, and S, consistent with enrichment from Type-II supernovae. These results demonstrate the importance of combining UV, optical, IR,

and X-ray observations to probe both obscured and unobscured star formation, the metal enrichment, and the outflow-driven evolution of starburst galaxies.

Keywords: galaxies: stars: formation – galaxies: individual (M 82) – ultraviolet: infrared: galaxies – starburst: galaxies – ISM: outflows – X-rays: galaxies

1 Introduction

The formation and evolution of galaxies is one of the most interesting phenomena in the universe, and the measurement of Star Formation Rate (SFR) provides important evidence for the investigation of the evolution of galaxies. The merging and interaction among galaxies provides intense starbursts in the cores of galaxies. Starburst galaxies typically have high star formation rates, and the measurement probes hot OB-type stars [1]. These youngest stellar populations in galaxies emit most of their energy in the Ultra-Violet (UV) band [2]. Therefore, imaging studies of such galaxies using high spatial resolution telescopes in far-ultra-violet (FUV) and near-ultra-violet (NUV) helps us to locate the active star-forming regions in galaxies. The UV radiation from hot OB stars, short-ward of the Lyman limit, ionised the surrounding gas to produce ionized hydrogen HII regions, and this ionized gas recombines and produces emission lines. As such, this recombination emission line flux provides an estimate of ionisation radiation in the H_α domain, which is commonly used to estimate the star formation rate.

The combination of feedback from supernovae ejecta with the material ejected from young massive stars in the surroundings results in the expanding bubbles around the super star clusters [3, 4]. The evolution of galaxies depends not only on the star formation process but also on the way the various feedback effects of star formation primarily influence the interstellar medium (ISM). The overall evolution of galaxies depends on the rate at which interstellar gas in the galaxies is converted into stars, and this efficiency of star formation depends on the rate at which diffuse interstellar matter is collected into star-forming regions.

X-ray observations expose an extended halo of soft X-ray emission around the majority of starburst galaxies [5–7]. In starburst galaxies, young massive stars inject metal-enriched gas and its kinetic energy into their surrounding medium through supernovae and stellar winds [8]. The high spatial resolution of observation facilities in the X-ray band such as *Chandra* and *XMM-Newton* provides the best facilities to study the spatial distribution of the temperature and metallicity of hot gas along these outflows [5, 6, 9–11].

The second largest galaxy in the Messier 81 (M 81) group, M 82 (also known as NGC 3034 or the Cigar galaxy) is a starburst galaxy with a large number of identified supernovae. The quintessential starburst galaxy, M 82 exhibits the superwind phenomenon [8, 12–17]. The massive ionised cloud in the halo of M 82 is the source of the X-ray emission, which is caused by shock heating [18]. [19] find a direct connection between the M 82 superwind and the warm-hot, metal-rich circumgalactic medium

(CGM). [20] highlights the close morphological association between the dust and the hotter phases of the winds investigated in H_α and the X-ray emission.

This study provides the first AstroSat Ultra-Violet Imaging Telescope (UVIT)-based spatially resolved SFR measurements combined with *Chandra* X-ray spectroscopy for M 82. The primary objective of this study is to identify the aggregations of the star-forming regions within the M 82 galaxy using FUV observations. Moreover, we can obtain the morphological correlation between different phases of the ISM by combining FUV, H_α , Mid-Infra Red (MIR) and X-ray observations. Lastly, we also determine the metal abundances from archival *Chandra* X-ray data of the M 82 galaxy.

This paper is structured as follows: Section 2 describes the data analysis techniques. In Section 3, results and its implications are presented. Lastly, Section 4 encapsulates the main findings.

For M 82 we adopt a more accurate luminosity distance of 3.53 Mpc from [21], rather than the distance listed in NASA/IPAC Extragalactic Database (NED)¹ for assumed cosmology, along with a unit conversion scale of $1'' = 17$ pc.

2 Observations and Data Reduction

M 82 is one of the nearest starburst galaxies at a redshift $z = 0.000897$ [22]. We observed M 82 (proposal ID : A04.222) galaxy using the Indian multi-wavelength astronomical satellite AstroSat [23]. Observations were carried out using UVIT onboard AstroSat along with the optical filter FUV (F148W). The observations were conducted on June 01, 2018, for a total exposure time of 388 seconds. The UVIT instrument has an impressive resolution of $\sim 1.2''$ for NUV and $\sim 1.4''$ for FUV channels. The UVIT consists of two telescopes that are co-aligned with diameters of 38 cm, one is dedicated to FUV observations and the other is used for observations in the NUV and visible channels. The photometric calibrations and details of UVIT instrumentation are found in [24–26].

The observed data was analysed and reduced by following the standard routine described in [25, 26]. The level-2 file was then obtained from the level-1 data by applying the UVIT level-2 Pipeline (UL2P) task. This thread consists of primary reduction, masking the bad pixels, flagging multi-photon event blocks, detecting cosmic-ray events, and finally correcting the drift to the event centroids. Then, multiple orbital images were combined after the astrometric correction. The final image was obtained in the form of an intensity map in units of counts per second. This paper uses only FUV(148W) band data sets, while other FUV data were rejected due to poor signal. Although we proposed the NUV for observation, the NUV observation was not possible due to observational limitations.

This paper also uses the archival X-ray data taken from *Chandra* space telescope on 24 June 2009 for 120 ks exposure (ObsID : 10542) and 1 July 2009 for 120 ks (ObsID : 10543). Both observations were carried out in a very faint mode (VFAINT) on the ACIS-S chip. The X-ray data were analysed using the standard method given by *Chandra* X-ray observatory analysis guide, and reprocessed by using Chandra Interactive Analysis of Observations (CIAO-4.11) software package. The analysis of the

¹<https://ned.ipac.caltech.edu/>

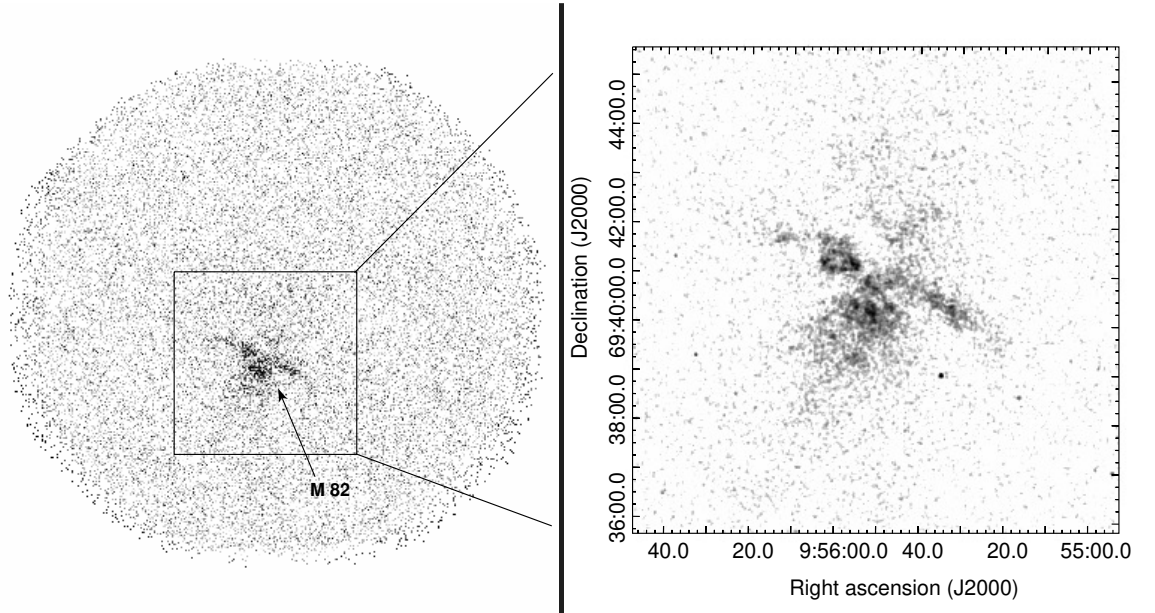


Fig. 1 AstroSat/UVIT images of the M 82 galaxy. The left panel image shows 28 arcmin diameter field of view and the right panel shows the zoomed in view covering a 10×10 arcmin² region.

X-ray data followed the procedures outlined in [27, 28]. Individual observational data were reprocessed from level-1 event files using the `chandra_repro` task and created the level-2 file. The level-2 file was then used to identify and remove the flares in the light curve if present in the observational data by using `deflare` script provided by CIAO. To improve the signal-to-noise level, the cleaned data of both the observations were merged by using `merge_obs` task. In the present study, we are interested only in the nature of the hot gas distribution, hence we identify and remove the resolved point sources detected by using the wavelet detection algorithm `wavdetect` task. The holes left behind after removal of point sources were filled by using the `dmfilth` task. Further these cleaned image is used for imaging and spectroscopic purpose.

3 Results and Discussion

3.1 Star formation in M 82

The left panel of Figure 1 shows the 28 arcmin diameter field of view image centred on the M 82 galaxy whereas the right panel of the figure shows a zoomed-in 10×10 arcmin² image of the galaxy, which was lightly Gaussian smoothed to suppress noise for better visualisation. The emission features of the warm FUV emitting gas in the M 82 galaxy is dominated by a biconical structure that defines the superwinds (i.e., looks like a butterfly). This indicates that the gas distribution is primarily along the minor axis (for more details, see Section 3.3).

The young (< 1 Gyr) massive hot star in galaxies emits most of its light in the UV region. Hence, the measurement of UV flux is a reasonable estimation of current/ongoing SFRs. This study uses FUV flux to estimate the star formation rate [29, 30] from the star formation region in the M 82 galaxy, assuming a constant SFR over the past 10^8 years.

$$\text{SFR}_{\text{FUV}} [M_{\odot} \text{ yr}^{-1}] = \frac{L_{\text{FUV}} [\text{erg s}^{-1}]}{3.83 \times 10^{33}} \times 10^{-9.51} \quad (1)$$

The net background subtracted counts (net count rate) were estimated by selecting the source and background regions independently. The source regions were selected by a visual inspection method as shown in Figure 2. The background counts were extracted from the source free regions which are far from the source and have similar region size to that of source. This count rate was further converted to flux density and flux using the unit conversion in the unit of $\text{erg cm}^{-2} \text{ s}^{-1} \text{ \AA}^{-1}$ as suggested in [25]. The obtained flux in the interested region was then converted to luminosity and finally to star formation rate. Figure 2 shows the regions of interest to estimate the SFR, and Table 1 reports the details of the estimated flux, luminosity, and SFRs in the selected regions. The total SFR in the M 82 galaxy was estimated by selecting the region up to where the FUV diffuse emission is visible (see Figure 2). The estimated value of total SFR for the radii of 3.6 kpc ($3.5'$) from the centre is $0.022 M_{\odot} \text{ yr}^{-1}$.

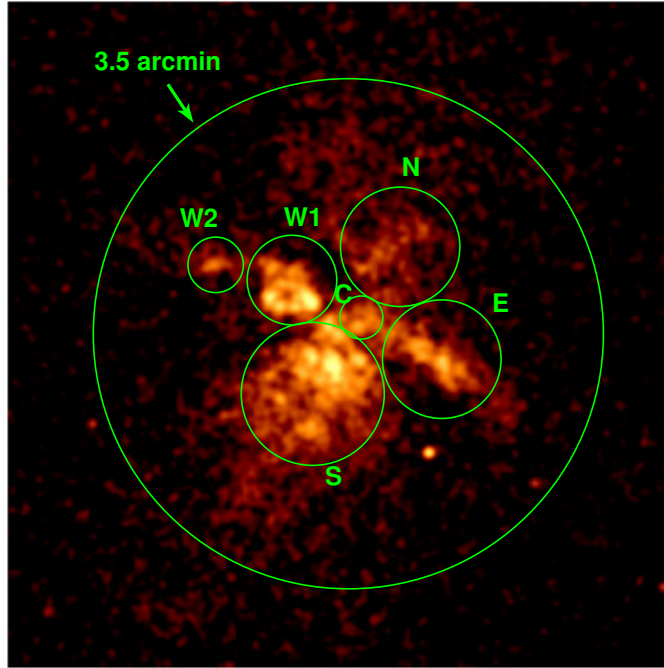


Fig. 2 The figure shows the FUV Gaussian smoothed image of M 82, with the regions where flux were estimated indicated using green circles.

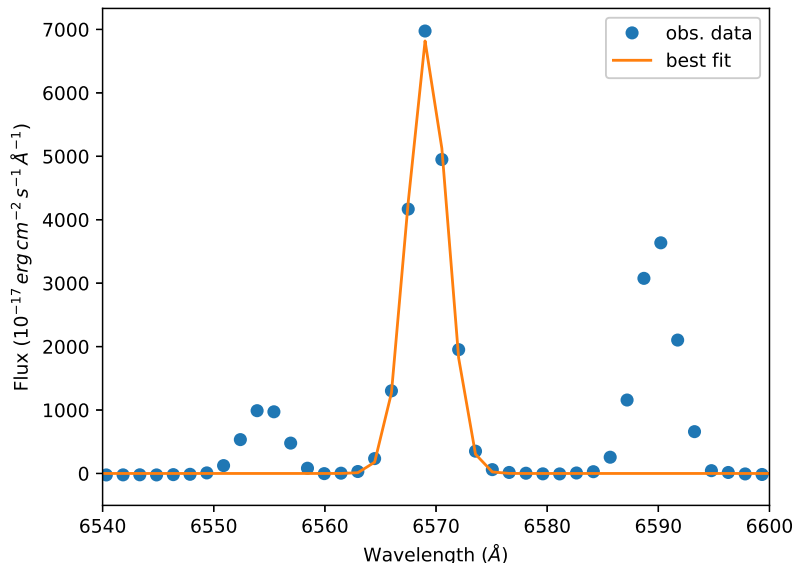


Fig. 3 SDSS continuum subtracted H_α emission fitted with Gaussian 1D model.

The young OB star clusters are surrounded by hydrogen gas. These young stars are hot enough to produce significant fluxes of ionising radiation. The HII region characterises the line emission; that is, the zone of ionised gas that emits the H_α . This allows us to directly convert H_α line emission into the star formation rate. Thus, the photo-ionisation rate can be expressed as hydrogen recombination line flux, and this relates to the SFR by assuming an electron temperature $T_e = 10^4$ K and by

$$\frac{\text{SFR}_{H_\alpha}}{M_\odot \text{ yr}^{-1}} = 5.37 \times 10^{-42} \left(\frac{L_{H_\alpha}}{\text{erg s}^{-1}} \right) \quad (2)$$

The relation above shows that the SFR is proportional to the H_α luminosity. The line emission flux is found using the SDSS spectra (Plate-1879; MJD-54478; FiberID-411). The SDSS-I/II fibre have a 3 arcsec diameter which covers 51 pc for M 82 galaxy. The H_α line emission flux emitted from core of M 82 galaxy is estimated by fitting a single Gaussian. The best-fit model parameters are amplitude = $2.99 \pm 0.04 \times 10^{-13}$ erg cm⁻² s⁻¹ Å⁻¹, central wavelength = 6569.19 ± 0.03 Å and equivalent width = 1.75 ± 0.02 Å. The best-fit model is shown in Figure 3. From this, we derive the H_α flux and find it to be 1.31×10^{-12} erg cm⁻² s⁻¹ for this SDSS fiber aperture. This corresponds to luminosity $L_{H_\alpha} = 1.95 \times 10^{39}$ erg s⁻¹ and SFR = $0.010 M_\odot \text{ yr}^{-1}$. [18] derived the total H_α flux for the entire region of M 82 as $\approx 4.6 \times 10^{-11}$ erg cm⁻² s⁻¹ hence the $L_{H_\alpha, \text{tot}} = 6.85 \times 10^{40}$ erg s⁻¹ this gives the total SFR $\sim 0.37 M_\odot \text{ yr}^{-1}$.

The infrared (IR) emission process of galaxies is dominated by different physical mechanisms. In particular, the mid-IR (5-25 μm) emissions are dominated by the warm dust emission process, which originates from the small size of dust grains which

Table 1 Luminosity and star formation rates estimated from the clumpy regions of the M 82 galaxy.

Regions	srcs-cnts (counts)	bkg-cnts (counts)	net-cnts (counts)	cnts×CF (10^{-15})	Flux (F) (10^{-11} erg s $^{-1}$ cm $^{-2}$)	$L = F \times 4\pi R^2$ (10^{40} erg s $^{-1}$)	SFR (M_{\odot} yr $^{-1}$)
Centre (C)	1.33	0.30	1.03	3.18	0.470	0.70	0.0006
North (N)	5.16	1.93	3.22	9.96	1.47	2.19	0.0018
South (S)	14.41	3.03	11.38	35.2	5.21	7.76	0.0063
East (E)	5.80	2.05	3.75	11.6	1.71	2.55	0.0021
West-1 (W1)	5.18	1.34	3.83	11.8	1.75	2.61	0.0021
West-2 (W2)	0.41	0.09	0.32	0.99	0.147	0.22	0.0002
Total	77.83	38.13	39.70	123.0	18.2	27.12	0.0220

Notes: srcs-cnts = source counts; bkg-cnts = background counts; net-cnts = background-subtracted source counts;
CF = conversion factor from counts to flux units (3.09×10^{-15}); Flux = cnts×CF× λ .

are heated by high energetic photons generated by young massive stars. Therefore, it is safe to assume that the IR emission is mostly powered by star formation [31]. However, recent studies show that the far-IR emission originates from star formation activities [32–35]. [32] estimate the SFR by measuring emission at $24\mu\text{m}$ that results from increasing the emission by warm dust heated by the young massive stars, over the cold dust heated by the radiation field. Further, we assume that the UV emission contribution to the total luminosity powered by young star is about 20%. Hence, the relation between SFR_{FIR} and FIR luminosity is given by [32]

$$\text{SFR}_{\text{FIR}} (M_{\odot} \text{yr}^{-1}) = (1.12 - 1.23) \times 10^{-9} L(24\mu\text{m}, L_{\odot}) \quad (3)$$

The $L(24\mu\text{m})$ luminosity is in units of L_{\odot} and derived from the $24\mu\text{m}$ flux, which was obtained from AKARI observations using the infrared camera (IRC) [36], and is reported in the NED database. The size of the aperture region (d) to estimate the flux is taken to be less than 4 arcmin. The $24\mu\text{m}$ flux of M 82 within the aperture region is $4.74 \times 10^{-8} \text{erg s}^{-1} \text{cm}^{-2}$, which corresponds to a luminosity of $1.46 \times 10^{10} L_{\odot}$, providing an estimate of the SFR_{FIR} of $\sim 16 - 18 M_{\odot} \text{yr}^{-1}$.

A significant difference is observed between the SFRs derived from FUV, $\text{H}\alpha$, and FIR emission. Also, the similar difference in values are obtained by [37] for sample of nearby galaxies. For M 82 the FUV and $\text{H}\alpha$ based estimates of $0.022 M_{\odot} \text{yr}^{-1}$ and $0.010 M_{\odot} \text{yr}^{-1}$, respectively, are considerably lower than the FIR-derived value of $16-18 M_{\odot} \text{yr}^{-1}$. This discrepancy arises because the FUV and $\text{H}\alpha$ tracers are highly sensitive to unobscured star formation and are significantly affected by dust attenuation, whereas the FIR emission primarily originates from dust heated by young massive stars, thereby tracing the dust-obscured component of star formation. Since M 82 is a prototypical dusty starburst galaxy, a substantial fraction of ongoing star formation is hidden from UV and optical observations but well captured in FIR observations. Additionally, no extinction corrections have been applied to the FUV and $\text{H}\alpha$ estimates in this study, which further contributes to their lower SFR values. Similar trends have been reported in previous studies (e.g., [31]; [32]), emphasising the need for multi-wavelength measurements to accurately quantify the total star formation rate in dusty starburst galaxies like M 82.

3.2 X-ray Spectroscopy

The protostarburst galaxy M 82, with its powerful superwind (Galactic-scale outflows), is a perfect target to study the driving plasma of superwinds [38]. Superwinds are important feedback processes in galaxy evolution that are driven by stellar winds from massive stars and core-collapse supernovae (SN) from active star-forming galaxies [38–40]. The superwinds will eject metals, which will enrich the halo gasses and intergalactic medium [41]. Hence, one of the primary indicators of the starburst phenomena is the X-ray emission.

Background subtracted, point source removed source spectra were used in XSPEC version: 12.9.0 [42] for spectral fitting. A circular region of 3.5 arcmin radius centred on the source position was used for spectral extraction. The multi-temperature variable abundance, along with the power-law model, was used to fit the extracted spectra simultaneously. We employed this model because both observational and simulation

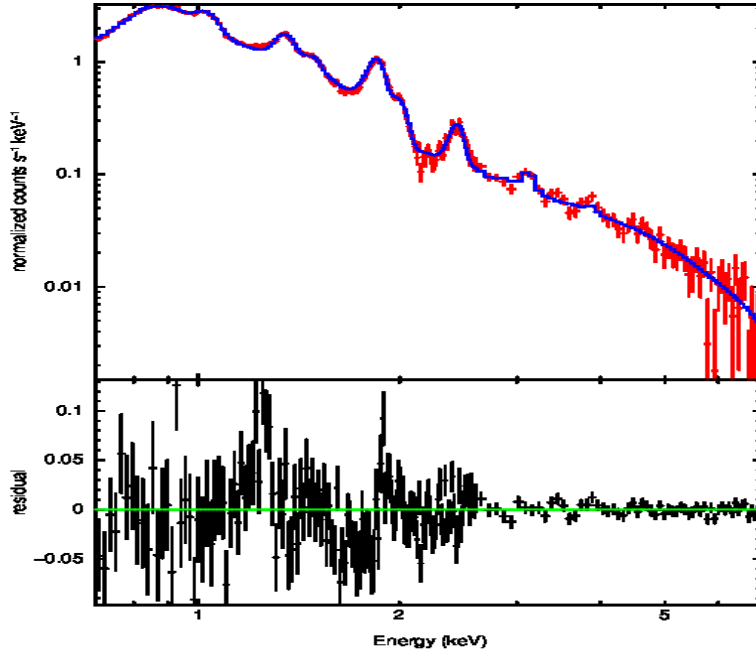


Fig. 4 *Chandra* X-ray spectrum of M 82 fitted with the best-fit model shown in blue. Bottom panel shows residual of the fit, illustrating the goodness of fit.

studies typically shows that the central region of starburst galaxies experience a multi-temperature gas phase, spanning from cold dust to hot outflows [43, 44].

A detailed X-ray spectroscopic study of the M 82 galaxy is presented in [19]. This model also includes two absorption components (PHABS): one is to account for the Galactic absorption along the direction of M 82, which was kept fixed at $N_H = 4.0 \times 10^{20} \text{ cm}^{-2}$ [45] and the other is for the intrinsic absorption which was allowed to vary. The variable collisional ionised plasma (VAPEC) model was used to estimate the temperature and metal abundance within the selected region. The power-law photon index was fixed at 1.5 to account for the unresolved sources present in that region. Thus the model used for spectral fitting of M 82: `phabs × phabs × (vapec + vapec + vapec + powerlaw)`. During the spectral fitting, all the temperatures kT_1 , kT_2 , and kT_3 and metal abundance Ne, Mg, Si, and S are allowed to vary, and other abundances were fixed at $0.5 Z_\odot$. The best-fit model parameters are shown in Table 2. The best spectral fit using this model yielded a reduced chi-square of ~ 1.35 ($\chi^2 / \text{dof} = 227/168$). The best-fitting spectrum is shown in Figure 4. The luminosity was estimated to be $2.44 \times 10^{40} \text{ erg s}^{-1}$.

We derived best-fit temperatures of $kT_1 \sim 0.22 \text{ keV}$, $kT_2 \sim 0.56 \text{ keV}$, and $kT_3 \sim 1.43 \text{ keV}$, indicating a multiphase, mass-loaded starburst driven wind. In particular, the 0.22 keV component displays a wider spread compared to the 0.56 keV and 1.43 keV plasmas [19]. The hottest phase ($kT_3 \sim 1.43 \text{ keV}$; $T \sim 1.7 \times 10^7 \text{ K}$) likely traces the recent supernova heated ejecta and the fast central wind material, while

Table 2 Spectral fit parameters

Parameter	Value
N_{H} (10^{20} cm $^{-2}$)	$38.0^{+0.06}_{-0.06}$
kT $_1$ (keV)	$0.22^{+0.05}_{-0.04}$
kT $_2$ (keV)	$0.56^{+0.15}_{-0.08}$
kT $_3$ (keV)	$1.43^{+0.45}_{-0.17}$
Ne (Z_{\odot})	$0.36^{+0.22}_{-0.36}$
Mg (Z_{\odot})	$0.86^{+0.06}_{-0.05}$
Si (Z_{\odot})	$0.89^{+0.93}_{-0.06}$
S (Z_{\odot})	$1.23^{+0.42}_{-0.19}$

N_{H} is the hydrogen column density. kT $_1$, kT $_2$, and kT $_3$ denote the plasma temperatures. Elemental abundances are given relative to the solar value.

the intermediate temperature component (kT $_2 \sim 0.56$ keV; $T \sim 6.5 \times 10^6$ K) represents shock heated ISM and mass-loaded gas at the base of the outflow. The coolest component (kT $_1 \sim 0.22$ keV; $T \sim 2.6 \times 10^6$ K) is consistent with cooled, entrained halo gas and possible interface emission between hot and cold phases [46]. The derived abundances indicate sub-solar neon (Ne $\sim 0.36 Z_{\odot}$) and nearly solar to slightly super-solar α -elements (Mg $\sim 0.86 Z_{\odot}$, Si $\sim 0.89 Z_{\odot}$, and S $\sim 1.23 Z_{\odot}$), suggesting that the hot gas is predominantly enriched by core-collapse supernovae (Type-II supernovae) associated with the ongoing starburst activity [47]. The relatively low neon abundance supports a young enrichment timescale, consistent with minimal contribution from intermediate mass stars [see 10, 48]. These results support a scenario in which hot, α -enhanced supernova ejecta interact with and mass-load the surrounding ISM, driving the multiphase bipolar outflow observed in M 82.

3.3 Multiphase ISM

M 82 is a galaxy that is currently experiencing an active starburst with significant outflow of material along its minor axis [19, 43, 49]. We can use the multi-wavelength observational imaging data to examine the association of ISM in the M 82 galaxy with other phases. For this, we derive the hot gas emission map, which is point sources subtracted, 0.5 - 3.0 keV Gaussian smoothed *Chandra* ACIS image of the M 82 galaxy, shown in the left panel of Figure 5. It is evident that the distribution of hot X-ray emitting gas is complex, abundant in the nuclear region, and significantly extended along the minor axis (North-South distance ~ 8.0 kpc) of the galaxy. Along the north side of the galaxy, the hot gas distribution displays a filamentary structure. The right panel of Figure 5 shows the Kitt Peak National Observatory (KPNO) *B*-band image extended along NW to SE direction shows the stellar emission is obscured by the interstellar dust. Figure 6 shows the 0.5 - 3 keV X-ray image, overlaid with continuum-subtracted H $_{\alpha}$ contours from the KPNO 2.1m archival observations in blue and FUV contours in red. Figure 6 illustrates a notable spatial correlation between the warm gas, traced by FUV and H $_{\alpha}$ emissions, and the hot gas, traced by soft X-ray emissions.

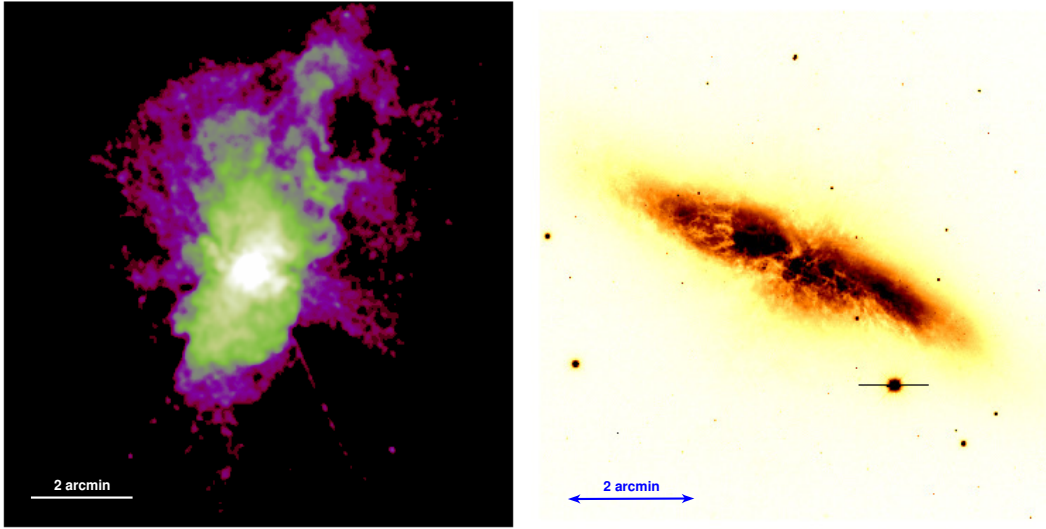


Fig. 5 Left panel: *Chandra* 0.5 - 3 keV background subtracted, exposure corrected smoothed X-ray image. Right panel: KPNO *B*-band optical image.

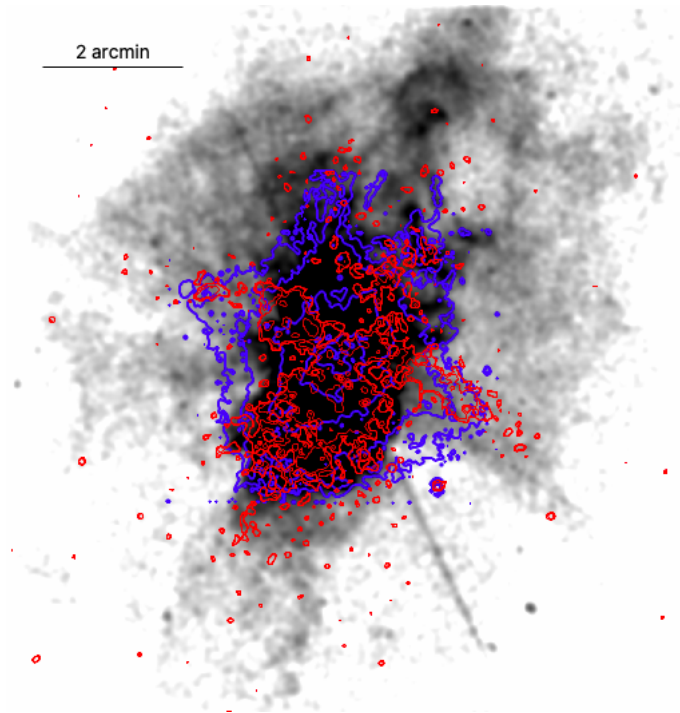


Fig. 6 *Chandra* X-ray image in the 0.5 - 3 keV energy band, overlaid with KPNO continuum subtracted H_{α} contours in blue and FUV contours in red.

This suggests that the multiphase ISM in M 82 is physically interconnected through a starburst-driven outflow. The emission from X-ray, FUV, and H_α are all extended in the minor axis direction. The alignment of these emissions along the minor axis, combined with significant dust obscuration along the major axis, supports the scenario of a bipolar superwind driven by starburst activity, which transports mass, energy, and metals from the central region to the halo and CGM.

4 Conclusion

In this work, we performed a multi-wavelength investigation of the starburst galaxy M 82 using UVIT FUV imaging and *Chandra* X-ray data, including both imaging and spectroscopy, to study its star-forming regions, hot gas distribution, and feedback driven outflows.

- The spatially-resolved FUV analysis identifies several star-forming knots, yielding a total SFR of $0.022 M_\odot \text{ yr}^{-1}$ within ~ 3.6 kpc.
- Comparison with H_α ($0.010 M_\odot \text{ yr}^{-1}$) and IR-derived ($16 - 18 M_\odot \text{ yr}^{-1}$) SFRs highlights that a significant fraction of star formation is hidden by dust.
- FUV, H_α , and soft X-ray emission exhibit a strong morphological correlation along the minor axis, tracing multi-phase outflows driven by intense star formation.
- X-ray spectral modelling indicates enhanced α -element abundances (Ne, Mg, Si, S), consistent with enrichment by Type-II supernovae in the starburst core.

These findings provide new insights into the multi-phase ISM and the role of stellar feedback in shaping the evolution of starburst galaxies. Future deep UVIT observations combined with integral field spectroscopy and high-resolution IR mapping will further clarify the interaction between star formation, outflows, and metal enrichment in M 82.

Acknowledgements. The authors are grateful to the anonymous referee for their careful reading and insightful comments. This research has made use of data obtained from AstroSat-UVIT observations, *Chandra* Archival observations, SDSS, and KPNO data. We also thank *Chandra* software provided by the *Chandra* X-ray Center (CXC) in the application packages CIAO and Sherpa. This paper also uses information from NASA extragalactic data centre (NED). The research work done at the Physical Research Laboratory, Ahmedabad, is funded by the Department of Space, Government of India. NV and MKP thanks to IUCAA, Pune, for providing the library facility.

References

- [1] Pearson, W. J. *et al.* Effect of galaxy mergers on star-formation rates. *A&A* **631**, A51 (2019).
- [2] Kennicutt, R. C. & Evans, N. J. Star Formation in the Milky Way and Nearby Galaxies. *ARA&A* **50**, 531–608 (2012).
- [3] Hartwell, J. M., Stevens, I. R., Strickland, D. K., Heckman, T. M. & Summers, L. K. *Chandra* and XMM-Newton observations of NGC 4214: the hot interstellar

- medium and the luminosity function of dwarf starbursts. *MNRAS* **348**, 406–420 (2004).
- [4] Levy, R. C. *et al.* JWST Observations of Starbursts: Massive Star Clusters in the Central Starburst of M82. *ApJ* **973**, L55 (2024).
- [5] Strickland, D. K., Heckman, T. M., Colbert, E. J. M., Hoopes, C. G. & Weaver, K. A. A High Spatial Resolution X-Ray and $H\alpha$ Study of Hot Gas in the Halos of Star-forming Disk Galaxies. I. Spatial and Spectral Properties of the Diffuse X-Ray Emission. *ApJS* **151**, 193–236 (2004).
- [6] Strickland, D. K., Heckman, T. M., Colbert, E. J. M., Hoopes, C. G. & Weaver, K. A. A High Spatial Resolution X-Ray and $H\alpha$ Study of Hot Gas in the Halos of Star-forming Disk Galaxies. II. Quantifying Supernova Feedback. *ApJ* **606**, 829–852 (2004).
- [7] Vagshette, N. D., Pandge, M. B., Pandey, S. K. & Patil, M. K. Dust extinction and X-ray emission from the starburst galaxy NGC 1482. *New A* **17**, 524–532 (2012).
- [8] Heckman, T. M., Armus, L. & Miley, G. K. On the Nature and Implications of Starburst-driven Galactic Superwinds. *ApJS* **74**, 833 (1990).
- [9] Rasmussen, J. & Ponman, T. J. XMM-Newton observations of two X-ray-bright galaxy groups - pushing out to r_{500} . *MNRAS* **349**, 722–734 (2004).
- [10] Tsuru, T. G. *et al.* X-Ray Spectral Study of the Extended Emission, ‘the Cap’, Located 11.6kpc above the Disk of M82. *PASJ* **59**, 269–282 (2007).
- [11] Ranalli, P., Comastri, A., Origlia, L. & Maiolino, R. A deep X-ray observation of M82 with XMM-Newton. *MNRAS* **386**, 1464–1480 (2008).
- [12] Axon, D. J. & Taylor, K. M82 - The exploding galaxy. *Nature* **274**, 37 (1978).
- [13] McCarthy, P. J., van Breugel, W. & Heckman, T. Evidence for Large-Scale Winds from Starburst Galaxies. I. The Nature of the Ionized Gas in M82 and NGC 253. *AJ* **93**, 264 (1987).
- [14] Bland, J. & Tully, B. Large-scale bipolar wind in M82. *Nature* **334**, 43–45 (1988).
- [15] Bregman, J. N., Schulman, E. & Tomisaka, K. High-Resolution X-Ray Imaging of the Starburst Galaxy M82. *ApJ* **439**, 155 (1995).
- [16] Strickland, D. K., Ponman, T. J. & Stevens, I. R. ROSAT observations of the galactic wind in M 82. *A&A* **320**, 378–394 (1997).
- [17] Shopbell, P. L. & Bland-Hawthorn, J. The Asymmetric Wind in M82. *ApJ* **493**, 129–153 (1998).

- [18] Lehnert, M. D., Heckman, T. M. & Weaver, K. A. Very Extended X-Ray and H α Emission in M82: Implications for the Superwind Phenomenon. *ApJ* **523**, 575–584 (1999).
- [19] Lopez, L. A., Mathur, S., Nguyen, D. D., Thompson, T. A. & Olivier, G. M. Temperature and Metallicity Gradients in the Hot Gas Outflows of M82. *ApJ* **904**, 152 (2020).
- [20] Hoopes, C. G. *et al.* GALEX Observations of the Ultraviolet Halos of NGC 253 and M82. *ApJ* **619**, L99–L102 (2005).
- [21] Karachentsev, I. D. The Local Group and Other Neighboring Galaxy Groups. *AJ* **129**, 178–188 (2005).
- [22] van der Tak, F. F. S., Aalto, S. & Meijerink, R. Detection of extragalactic H $_3$ O $^+$. *A&A* **477**, L5–L8 (2008).
- [23] Agrawal, P. C. A broad spectral band Indian Astronomy satellite ‘Astrosat’. *Advances in Space Research* **38**, 2989–2994 (2006).
- [24] Tandon, S. N., Ghosh, S. K., Hutchings, J., Stalin, C. S. & Subramaniam, A. Ultraviolet Imaging Telescope on AstroSat. *Current Science* **113**, 583 (2017).
- [25] Tandon, S. N. *et al.* In-orbit Performance of UVIT and First Results. *Journal of Astrophysics and Astronomy* **38**, 28 (2017).
- [26] Tandon, S. N. *et al.* In-orbit Calibrations of the Ultraviolet Imaging Telescope. *AJ* **154**, 128 (2017).
- [27] Vagshette, N. D., Naik, S. & Patil, M. K. Cavities, shocks and a cold front around 3C 320. *MNRAS* **485**, 1981–1989 (2019).
- [28] Kyadampure, A., Vagshette, N. D. & Patil, M. K. X-ray Cavities in the G50 Bright Group-Centered Galaxy NGC 5846. *Serbian Astronomical Journal* **202**, 17–24 (2021).
- [29] Iglesias-Páramo, J. *et al.* Star Formation in the Nearby Universe: The Ultraviolet and Infrared Points of View. *ApJS* **164**, 38–51 (2006).
- [30] Cortese, L., Gavazzi, G. & Boselli, A. The ultraviolet luminosity function and star formation rate of the Coma cluster. *MNRAS* **390**, 1282–1296 (2008).
- [31] Kennicutt, J., Robert C. Star Formation in Galaxies Along the Hubble Sequence. *ARA&A* **36**, 189–232 (1998).
- [32] Rieke, G. H. *et al.* Determining Star Formation Rates for Infrared Galaxies. *ApJ* **692**, 556–573 (2009).

- [33] Hatziminaoglou, E. *et al.* HerMES: Far infrared properties of known AGN in the HerMES fields. *A&A* **518**, L33 (2010).
- [34] Kirkpatrick, A. *et al.* GOODS-Herschel: Impact of Active Galactic Nuclei and Star Formation Activity on Infrared Spectral Energy Distributions at High Redshift. *ApJ* **759**, 139 (2012).
- [35] Feltre, A. *et al.* The roles of star formation and AGN activity of IRS sources in the HerMES fields. *MNRAS* **434**, 2426–2437 (2013).
- [36] Kaneda, H. *et al.* Large-scale distributions of mid- and far-infrared emission from the center to the halo of M 82 revealed with AKARI. *A&A* **514**, A14 (2010).
- [37] Kennicutt, R. C., Jr. *et al.* Dust-corrected Star Formation Rates of Galaxies. I. Combinations of H α and Infrared Tracers. *ApJ* **703**, 1672–1695 (2009).
- [38] Liu, J., Gou, L., Yuan, W. & Mao, S. Fe K lines in the nuclear region of M82. *MNRAS* **437**, L76–L80 (2014).
- [39] Heckman, T. M. *et al.* An X-Ray and Optical Study of the Dwarf Galaxy NGC 1569: Evidence for a Starburst-driven Outflow. *ApJ* **448**, 98 (1995).
- [40] Veilleux, S., Cecil, G. & Bland-Hawthorn, J. Galactic Winds. *ARA&A* **43**, 769–826 (2005).
- [41] Tumlinson, J. *et al.* The Large, Oxygen-Rich Halos of Star-Forming Galaxies Are a Major Reservoir of Galactic Metals. *Science* **334**, 948 (2011).
- [42] Arnaud, K., Borkowski, K. J. & Harrington, J. P. X-Ray Emission from the Wind-blown Bubble in the Planetary Nebula BD +30 degrees 3639. *ApJ* **462**, L75 (1996).
- [43] Leroy, A. K. *et al.* The Multi-phase Cold Fountain in M82 Revealed by a Wide, Sensitive Map of the Molecular Interstellar Medium. *ApJ* **814**, 83 (2015).
- [44] Li, X.-F., Zhu, W., Wang, T.-R. & Feng, L.-L. Revisiting the Galactic Winds in M82. II. Development of Multiphase Outflows in Simulations. *ApJ* **982**, 28 (2025).
- [45] Dickey, J. M. & Lockman, F. J. H I in the galaxy. *ARA&A* **28**, 215–261 (1990).
- [46] Porraz Barrera, N. *et al.* Hot Gas Outflow Properties of the Starburst Galaxy NGC 4945. *ApJ* **968**, 54 (2024).
- [47] Mitsuishi, I., Yamasaki, N. Y. & Takei, Y. An X-Ray Study of the Galactic-Scale Starburst-Driven Outflow in NGC 253. *PASJ* **65**, 44 (2013).
- [48] Fukushima, K., Kobayashi, S. B. & Matsushita, K. Revisiting the abundance

pattern and charge-exchange emission in the centre of M 82. *A&A* **686**, A96 (2024).

- [49] Lopez, S., Lopez, L. A., Thompson, T. A., Leroy, A. K. & Bolatto, A. D. Observational Constraints on Cool Gas Clouds in M82's Starburst-driven Outflow. *ApJ* **989**, 100 (2025).